Experimental Validation of Nonlinear Adaptive Sliding Mode Control on a One-Degree-Of-Freedom Helicopter System

Samuel E. Newport*, Dr. Farbod Fahimi†, and Dr. Richard Tantaris‡
University of Alabama in Huntsville, Huntsville, AL, 35899, United States

This work presents experimental validation of a nonlinear adaptive sliding mode control (NASMC) architecture on the Quanser Aero, a two-degree-of-freedom (2DOF) helicopter test platform. The NASMC control law and associated parameter adaptation rules were implemented in MATLAB/Simulink and deployed to both a nonlinear simulation model and physical hardware. Simulation results demonstrate accurate trajectory tracking and convergence of adaptive parameter estimates. Hardware validation was conducted by isolating each rotational axis and independently testing the pitch and yaw control. In these single-degree-of-freedom (1DOF) experiments, the NASMC controller achieved stable tracking of the commanded trajectories and convergence of adaptation parameters. Performance was compared against the baseline linear quadratic regulator (LQR) controller provided with the Quanser Aero Platform. The NASMC control architecture demonstrated improved tracking of commanded pitch and yaw commands, demonstrating the feasibility of deploying the NASMC on Aerospace hardware. Ongoing work should characterize the gain sensitivity of the control architecture and demonstrate its performance on systems with higher degrees of freedom.

I. Nomenclature

θ	=	pitch rotation about the $+y$ axis
$\dot{\theta}$	=	angular rate about the $+y$ axis
$\ddot{\theta}$	=	angular acceleration about the $+y$ axis
ψ	=	yaw rotation about the $+z$ axis
$\dot{\psi}$	=	angular rate about the $+z$ axis
$\ddot{\psi}$	=	angular acceleration about the $+z$ axis
a_p	=	unknown system parameters associated with pitch dynamics
a_y	=	unknown system parameters associated with yaw dynamics
$\tilde{a_p}$	=	parameter estimation error for parameters associated with pitch dynamics
$\tilde{a_y}$	=	parameter estimation error for parameters associated with yaw dynamics
α_p	=	unknown system parameters associated with pitch dynamics (alternative form of a_p)
α_y	=	unknown system parameters associated with yaw dynamics (alternative form of a_y)
b_p	=	unknown system parameter for pitch dynamics
b_y	=	unknown system parameter for yaw dynamics
γ_i	=	controller gain
e	=	output tracking error
η	=	gain for sliding mode surface reaching phase
D_p	=	viscous pitch damping coefficient
D_y	=	viscous yaw damping coefficient
δ	=	disturbance term
f_i	=	known functions of state and time
g	=	acceleration of gravity
h_p	=	unknown system parameter for pitch dynamics (alternative form of b_p)
h_y	=	unknown system parameter for yaw dynamics (alternative form of b_y)

*Undergraduate Student, Department of Mechanical and Aerospace Engineering, AIAA University Student Member 1405596.
†Associate Professor, Department of Mechanical and Aerospace Engineering
‡Clinical Assistant Professor, Department of Mechanical and Aerospace Engineering

$\tilde{h}_p$ = parameter estimation error of h_p
$\tilde{h}_y$ = parameter estimation error of h_y
J_p = pitch axis moment of inertia
J_y = yaw axis moment of inertia
k = gain for sliding mode surface reaching phase
λ = gain for sliding mode surface sliding phase
m = mass of pivot
ρ = residual error
s = combined error
s_Δ = modified combined error
t = time
u = control input
$u_{p,F}$ = primary virtual control input for control of pitch dynamics
$u_{y,R}$ = primary virtual control input for control of yaw dynamics
$v_{p,F}$ = secondary virtual control inputs for control of pitch dynamics and front fan
$v_{y,R}$ = secondary virtual control inputs for control of yaw dynamics and rear fan
V_1 = motor voltage inputs for front fan
V_0 = motor voltage inputs for rear fan
V = Lyapunov function
y = arbitrary state variable
ϕ_s = boundary layer thickness
ω_F = front fan, providing pitch-thrust, angular speed
ω_R = rear fan, providing yaw-thrust, angular speed
d_1 = distance from the geometric center of the pivot to the geometric center of the front fan
d_0 = distance from the geometric center of the pivot to the geometric center of the rear fan
d_{cm} = distance from the geometric center of the pivot to the center of mass of the pivot
F_0 = thrust from the front fan
F_1 = thrust from the rear fan
τ_p = net torque about the pitch axis ($+y$ axis)
τ_y = net torque about the yaw axis ($+z$ axis)
K_{F1} = coefficient relating the front motor angular rate, Ω_F, to the front motor's thrust, F_F
K_{F0} = coefficient relating the rear motor angular rate, Ω_F, to the rear motor's thrust, F_R
$K_{M1,1}$ = first-order term coefficient relating the front motor angular rate, Ω_F, to the torque about the yaw axis, τ_y
$K_{M1,2}$ = second-order term coefficient relating the front motor angular rate, Ω_F, to the torque about the yaw axis, τ_y
$K_{M0,1}$ = first-order term coefficient relating the rear motor angular rate, Ω_R, to the torque about the pitch axis, τ_p
$K_{M0,2}$ = second-order term coefficient relating the rear motor angular rate, Ω_R, to the torque about the pitch axis, τ_y

II. Introduction

Former University of Alabama in Huntsville master's student Ryan Mathewson proposed a theoretical framework for the application of Nonlinear Adaptive Sliding Mode Control (NASMC) to quadcopter systems [1]. Building on this work, the present study seeks to transition NASMC from theory to practice by deploying a reformulated version of the approach on the Quanser Aero testbed, thereby demonstrating its effectiveness on physical hardware representing aerospace systems.

The Quanser Aero platform, which resembles a helicopter with coupled pitch and yaw dynamics, provides a representative test case. Currently, there are limited adaptive control studies specifically targeting helicopters and UAVs [2]. Meanwhile, model-free adaptive control methods, such as those based on machine learning, face barriers to implementation due to the difficulty of guaranteeing stability and robustness, as highlighted by the FAA [3]. This underscores the demand for approaches like NASMC, which are grounded in rigorous stability theory but require experimental verification.

This research will experimentally evaluate NASMC on the Quanser Aero, quantifying its stability, robustness, and safety. The results will bridge the gap between theoretical development and practical application, supporting the broader integration of adaptive control strategies into digital engineering frameworks for future aerospace and defense systems.

III. Background

The NASMC techniques deployed to hardware were taken from the second-order system derivation presented in [1]; however, the techniques used can be applied to any number order system. The techniques derived and used in [1] for a second and fourth-order system were originally derived from Slotine's and Li's work in [4] as well as Slotine's and Coetsee's work in [5]. A brief derivation of a general second-order system is provided here for convenient reference; please refer to the references mentioned previously for a more detailed derivation for systems of any order.

To design a controller for a second-order system, consider the following dynamic equation:

$$\ddot{y} + \alpha_1 f_1 + \alpha_2 f_2 = bu + \delta \tag{1}$$

where $\ddot{y}$ is the second derivative of position with respect to time, $u(t)$ is the control input, δ is the disturbance term, the f_i terms are known non-linear functions of the state and time, and α and $b \neq 0$ are unknown system parameters. Solving Eq. (1) for the control variable yields

$$h\ddot{y} + a_1 f_1 + a_2 f_2 + d = u \tag{2}$$

where $h = 1/b$, $a_i = \alpha_i/b$, and $d = -\delta/b$ for convenience. We define s as the combined error:

$$s = \dot{y} - \dot{y}_r \tag{3}$$

where $\dot{y}_r$ is the reference value defined as:

$$\dot{y}_r = \dot{y}_d - \lambda e \tag{4}$$

where $e = y - y_d$ is the output tracking error. The gain λ will drive the error to zero exponentially for any $\lambda > 0$. A control law is proposed in Eq. (5) assuming known system parameters:

$$u = h\ddot{y}_r - ks + a_1 f_1 + a_2 f_2 \tag{5}$$

where k is chosen as a constant of the same sign as h and the reference value, $\ddot{y}_r$, for the second derivative of position, $\ddot{y}$, is defined as:

$$\ddot{y}_r = \ddot{y}_d - \lambda\dot{e} \tag{6}$$

The control law proposed in Eq. (5) is revised to include the estimated values of the system parameters. Estimated parameters are indicated using hat notation (i.e., h is a known system parameter; while, $\hat{h}$ is an estimated system parameter):

$$u = \hat{h}\ddot{y}_r - ks + \hat{a}_1 f_1 + \hat{a}_2 f_2 \tag{7}$$

To design the adaptation laws for the estimated parameters, a Lyapunov function candidate, V, is defined as:

$$V = \frac{1}{2}(s_\Delta^2 + b((\frac{\hat{h} - h}{\gamma_0})^2 + (\frac{\hat{a}_1 - a_1}{\gamma_1})^2 + (\frac{\hat{a}_2 - a_2}{\gamma_2})^2)) \tag{8}$$

where $\hat{h}$ and $\hat{a}_i$ are the estimated values of h and a_i respectively, and γ_i are the tuning gains. Before moving forward with the adaptation law derivation, a saturation function is introduced effectively creating a boundary layer about $s = 0$:

$$sat(s/\phi_s) = \begin{cases} -1, & s \leq -\phi_s \\ s/\phi_s, & -\phi_s < s < \phi_s \\ 1, & s \geq \phi_s \end{cases} \tag{9}$$

using Eq. (9), the distance from the current state to the boundary layer, s_Δ, is defined as:

$$s_\Delta = s - \phi_s \mathrm{sat}(s/\phi_s) \tag{10}$$

Now, we continue by selecting the control law u as:

$$u = \hat{a}_1 f_1 + \hat{a}_2 f_2 + \hat{h}\ddot{y}_r - \hat{h}(D + \eta)\mathrm{sat}(s/\phi_s) \tag{11}$$

Here, we have substituted ks from Eq. (7) for $\hat{h}(D + \eta)\mathrm{sat}(s/\phi_s)$; where D is the maximum disturbance and η is the gain for the sliding mode surface reaching phase. Finally, the adaptation laws are selected as:

$$\dot{\hat{h}} = \gamma_0^2 s_\Delta(\ddot{y}_r + (D + \eta)\mathrm{sat}(s/\phi_s)) \tag{12}$$

$$\dot{\hat{a}}_1 = -\gamma_1^2 f_1 s_\Delta \tag{13}$$

$$\dot{\hat{a}}_2 = -\gamma_2^2 f_2 s_\Delta \tag{14}$$

Thus, the derivative of the Lyaponuv function, $\dot{V}$, is always negative. This means that V will reach a constant minimum, ultimately resulting in no residual error.

The following proof demonstrates how selection of these adaptation laws, Eqs. (12)-(14), leads to a monotonically negative $\dot{V}$. We start by taking the derivative of Eq. (3):

$$\dot{s} = \ddot{y} - \ddot{y}_r \tag{15}$$

By substituting Eq. (1), Eq. (6), and Eq. (11) into Eq. (15) we get:

$$\dot{s} = (\hat{a}_1 - a_1)bf_1 + (\hat{a}_2 - a_2)bf_2 - (b\hat{h} - 1)\ddot{y}_r - b\hat{h}(D + \eta)\mathrm{sat}(s/\phi_s) + d \tag{16}$$

Noting that $\dot{s}_\Delta = \dot{s}$ outside the boundary layer and $s_\Delta = 0$ inside the boundary layer, taking the time derivative of the Lyaponuv function, Eq. (8), yields:

$$\dot{V}(t) = \dot{s}s_\Delta + b\left(\frac{\dot{\hat{h}}}{\gamma_0^2}(\hat{h} - h) + \frac{\dot{\hat{a}}_1}{\gamma_1^2}(\hat{a}_1 - a_1) + \frac{\dot{\hat{a}}}{\gamma_2^2}(\hat{a}_2 - a_2)\right) \tag{17}$$

Substituting the $\dot{s}$ term from Eq. (16) into Eq. (17) gives:

$$\begin{aligned}\dot{V} = (b\hat{h} - 1)\left(\frac{\dot{\hat{h}}}{\gamma_0^2} - \ddot{y}_r s_\Delta\right) + \tilde{a}_1 b\left(\frac{\dot{\hat{a}}_1}{\gamma_1^2} + f_1 s_\Delta\right) + \tilde{a}_2 b\left(\frac{\dot{\hat{a}}_2}{\gamma_2^2} + f_2 s_\Delta\right)\\ - b\hat{h}(D + \eta)s_\Delta \mathrm{sat}(s/\phi_s) + ds_\Delta\end{aligned} \tag{18}$$

with the selected adaptation laws Eqs. (12)-(14), Eq. (18) simplifies to:

$$\dot{V} = (-(D + \eta)\mathrm{sat}(s/\phi_s) + d)s_\Delta \tag{19}$$

Eq. (19) further simplifies when outside of the boundary layer to:

$$\dot{V} \leq -\eta|s_\Delta| \tag{20}$$

Thus, by Eq. (20), it is shown that $\dot{V}$ is monotonically negative because we choose $\eta > 0$. The reader is encouraged to review [1] for a more detailed derivation.

IV. Methodology

The Quanser Aero, a 2 degree of freedom (DOF) helicopter platform [6], was selected to experimentally validate the NASMC controller. The following steps were taken to design and deploy the controller:

1) Bench tests to understand the Quanser Aero system's behavior (ie. establish sign conventions).

2) Determined the Quanser Aero's equations of motion

3) Derived a control law from the equations of motion and the general forms shown in Eqs. (11)-(14)

4) Tuned controller gains using a MATLAB/Simulink model

5) Deployed controller to the Quanser aero platform

A. Coordinate System and Hardware Setup

The Quanser Aero was connected to a Simulink model where scopes displayed the live pitch and yaw values. The platform was rotated by hand about the pitch and yaw axes to determine the positive and negative directions measured by the hardware. The coordinate system is shown in Fig. 1.

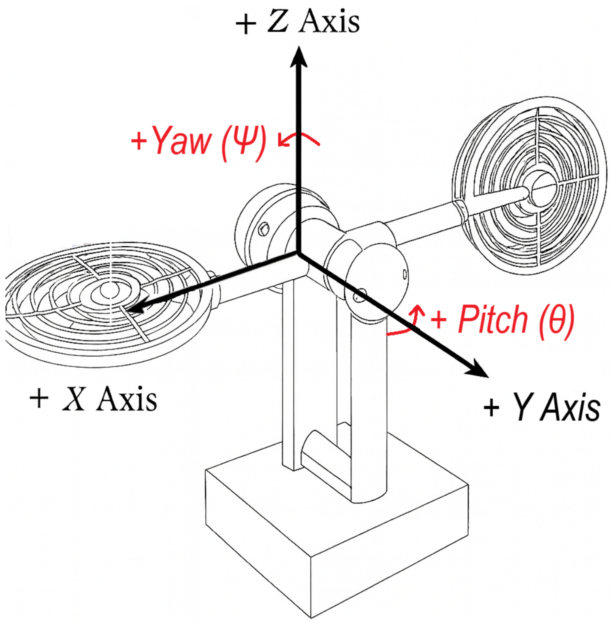

Fig. 1 Quanser Aero adapted from [6] with a coordinate system added to define the positive pitch and yaw axes

B. Quanser Aero Equations of Motion

After defining a coordinate system, a sign convention was determined to establish a relationship between motor voltage, motor angular speed, and reaction torques. The sign conventions are defined in Table 1, while Fig. 2 completes the defined sign conventions, depicting the motors and the corresponding subscripts 0 and 1.

Table 1 Quanser Aero dynamic model sign conventions

Applied Voltage $[V]$	Motor Speed $[rad/s]$	Thrust Effect $[rad]$	Torque Effect $[rad]$
$V_0 > 0$	$\omega_0 > 0$	$\dot{\psi} < 0$	$\dot{\theta} > 0$
$V_1 > 0$	$\omega_1 > 0$	$\dot{\psi} > 0$	$\dot{\theta} > 0$

With a coordinate system and sign conventions defined, we move forward by deriving the equations of motion. Starting with pitch dynamics, the general form of the sum of the torques is:

$$\tau_p = \tau_{F,p} + \tau_{M,p} - \tau_{v,p} - \tau_{mg} \tag{21}$$

The torques considered for the pitch dynamics are defined as:

$$\tau_p = J_p\ddot{\theta} \tag{22}$$
$$\tau_{F,p} = \omega_1^2 K_{F1} d_1 \tag{23}$$
$$\tau_{M,p} = \omega_0 K_{M0,1} + \omega_0^2 K_{M0,2} \tag{24}$$
$$\tau_{v,p} = D_p\dot{\theta} \tag{25}$$
$$\tau_{mg} = mgd_{cm}sin(\theta) \tag{26}$$

The constant K_{F1} maps the angular speed of motor 1, ω_1, to a thrust force; the constant d_1, the distance from the pivot to the center of the motor, relates this thrust force to a pitch moment. The constants $K_{M0,1}$ and $K_{M0,2}$ map the angular speed of motor 0, ω_0, to a reaction pitch moment.

For yaw dynamics, the general form of the sum of the torques is:

$$\tau_y = -\tau_{F,y} + \tau_{M,y} - \tau_{v,y} \tag{27}$$

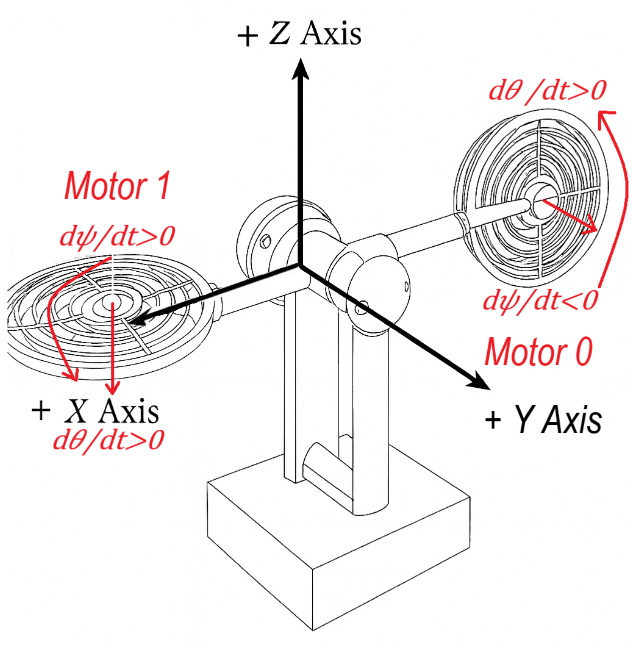

Fig. 2 Quanser Aero adapted from [6] with added sign conventions for forces and moments

The torques considered for yaw dynamics are defined as:

$$\tau_y = J_y\ddot{\psi} \tag{28}$$

$$\tau_{F,y} = \omega_0^2 K_{F0} d_0 \tag{29}$$

$$\tau_{M,y} = \omega_1 K_{M1,1} + \omega_1^2 K_{M1,2} \tag{30}$$

$$\tau_{v,y} = D_y\dot{\psi} \tag{31}$$

The constant K_{F0} maps the angular speed of motor 0, ω_0, to a thrust force; the constant d_0, the distance from the pivot to the center of the motor, relates this thrust force to a yaw moment. The constants $K_{M1,1}$ and $K_{M1,2}$ map the angular speed of motor 1, ω_1, to a reaction yaw moment.

Motor speed and voltage are related as follows:

$$\omega_i^2 = (K_{vi}V_i)^2 \tag{32}$$

where the subscript i refers to motor 0 or motor 1 and the constant K_{vi} relates the voltage to an angular rate.

By combining the pitch equations, Eq. (21)-(26), and then the yaw equations, Eq. (27)-(31), the system dynamics were defined as:

$$\ddot{\theta} = (\omega_1^2 K_{F1} d_1 + \omega_0 K_{M0,1} + \omega_0^2 K_{M0,2} - D_p\dot{\theta} - mgd_{cm}sin(\theta))/J_p \tag{33}$$

$$\ddot{\psi} = (-\omega_0^2 K_{F0} d_0 + \omega_1 K_{M1,1} + \omega_1^2 K_{M1,2} - D_y\dot{\psi})/J_y \tag{34}$$

Finally, after substituting in Eq. (32) into Eqs. (33)-(34):

$$\ddot{\theta} = (V_1^2 K_{v1}^2 K_{F1} d_1 + \omega_0 K_{M0,1} + \omega_0^2 K_{M0,2} - D_p\dot{\theta} - mgd_{cm}sin(\theta))/J_p \tag{35}$$

$$\ddot{\psi} = (-V_0^2 K_{v0}^2 K_{F0} d_0 + \omega_1 K_{M1,1} + \omega_1^2 K_{M1,2} - D_y\dot{\psi})/J_y \tag{36}$$

C. Quanser Aero Control Law

To derive the pitch control and adaptation laws, we begin by solving for the control variable. The control variable V_1^2, input voltage to motor 1, was selected to match the general form of the controller as shown in Eq. (2).

$$V_1^2 = \frac{J_p}{K_{v1}^2 K_{F1} d_1}\ddot{\theta} + \frac{D_p}{K_{v1}^2 K_{F1} d_1}\dot{\theta} + \frac{mgd_{cm}}{K_{v1}^2 K_{F1} d_1}sin(\theta) - \frac{K_{M0,1}}{K_{v1}^2 K_{F1} d_1}\omega_0 - \frac{K_{M0,2}}{K_{v1}^2 K_{F1} d_1}\omega_0^2 \tag{37}$$

Comparing Eqs. (1)-(2) with Eq. (37), the coefficients, α and a, and the functions of the states variables, f_i, are tabulated in Table 2.

Table 2 Pitch control law coefficients

$b = \frac{K_{v1}^2 K_{F1} d_1}{J_p}$	$h = \frac{J_p}{K_{v1}^2 K_{F1} d_1}$	$\ddot{y} = \ddot{\theta}$	$u = V_1^2$
$\alpha_1 = \frac{D_p}{J_p}$	$a_1 = \frac{D_p}{K_{v1}^2 K_{F1} d_1}$	$f_1 = \dot{\theta}$	
$\alpha_2 = \frac{mgd_{cm}}{J_p}$	$a_2 = \frac{mgd_{cm}}{K_{v1}^2 K_{F1} d_1}$	$f_2 = sin(\theta)$	
$\alpha_3 = \frac{-K_{M0,1}}{J_p}$	$a_3 = \frac{-K_{M0,1}}{K_{v1}^2 K_{F1} d_1}$	$f_3 = \omega_0$	
$\alpha_4 = \frac{-K_{M0,2}}{J_p}$	$a_4 = \frac{-K_{M0,2}}{K_{v1}^2 K_{F1} d_1}$	$f_4 = \omega_0^2$	

The derivation is repeated for the yaw control and adaptation laws. Solving for the yaw control variable, V_0^2, yields:

$$-V_0^2 = \frac{J_y}{K_{v0}^2 K_{F0} d_0}\ddot{\psi} + \frac{D_y}{K_{v0}^2 K_{F0} d_0}\dot{\psi} - \frac{K_{M1,1}}{K_{v0}^2 K_{F0} d_0}\omega_1 - \frac{K_{M1,2}}{K_{v0}^2 K_{F0} d_0}\omega_1^2 \tag{38}$$

Comparing Eqs. (1)-(2) with Eq. (38), the coefficients, α and a, and the functions of the states variables, f_i, are tabulated in Table 3.

Table 3 Yaw control law coefficients

$b = \frac{K_{v0}^2 K_{F0} d_0}{J_y}$	$h = \frac{J_y}{K_{v0}^2 K_{F0} d_0}$	$\ddot{y} = \ddot{\psi}$	$u = V_0^2$
$\alpha_1 = \frac{D_y}{J_y}$	$a_1 = \frac{D_y}{K_{v0}^2 K_{F0} d_0}$	$f_1 = \dot{\psi}$	
$\alpha_2 = \frac{-K_{M1,1}}{J_y}$	$a_2 = \frac{-K_{M1,1}}{K_{v0}^2 K_{F0} d_0}$	$f_2 = \omega_1$	
$\alpha_3 = \frac{-K_{M1,2}}{J_y}$	$a_3 = \frac{-K_{M1,2}}{K_{v0}^2 K_{F0} d_0}$	$f_3 = \omega_1^2$	

The parameters h and a in Table 2 and Table 3 are the known nominal values for pitch and yaw, respectively. Note that knowledge of these parameters is not necessary as the adaptation laws defined in Eqs. (12)-(14) will provide the estimates $\hat{h}_i$ and $\hat{a}_i$.

D. Simulation

The NASMC controller was applied to the Quanser Aero system using the dynamic equations of motion, control law, and adaptation laws defined in the preceding sections. The dynamic model and the controller implementation were created in Simulink and then ran from a MATLAB script to initialize parameters and plot the results. A high level overview of the Simulink model is given by Fig. 3

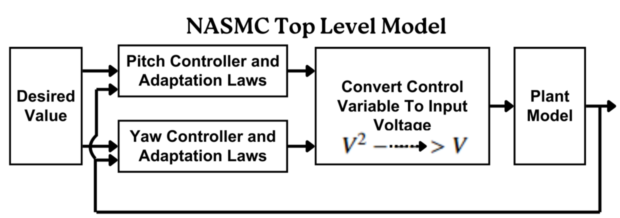

Fig. 3 High level overview of NASMC Simulink model

The simulation was used to tune the controller gains before deploying the control architecture to the hardware. The system parameters used to define the plant model were taken from [7]. While nominal, or truth, parameters were used to define the plant model, the controller was initialized by randomly drawing the initial parameter guesses between one-tenth and ten times the nominal values. For example, the initial guess for $\hat{h}_i$ was drawn from $\hat{h}_i = h[0.1 + (10 - 0.1)\text{rand}()]$. Thus, demonstrating that the controller does not require knowledge of the system parameters. Note that the simulation results of the MATLAB/Simulink model, controlled using NASMC, showed stable convergence for all degrees of freedom. These simulated results are not presented in this paper, due to space limitations.

V. Experimental Results

The experimentation was conducted one-degree-of-freedom (1DOF) at a time; to test the controller performance for a pitch command, the yaw axis was locked; to test the controller performance for a yaw command, the pitch axis was locked. Note that testing the controller 1DOF at a time results in zero coupling effects. Thus, the omega terms, ω_0 and ω_1, in Eq. (37)-(38), are zero and the associated coefficients do not adapt. The gains used for experimentation are summarized in Table 4.

	$\boldsymbol{\lambda}$	$\boldsymbol{D}$	$\boldsymbol{\eta}$	$\boldsymbol{\phi_s}$	$\boldsymbol{\gamma_0}$	$\boldsymbol{\gamma_1}$	$\boldsymbol{\gamma_2}$	$\boldsymbol{\gamma_3}$	$\boldsymbol{\gamma_4}$
Pitch Value	10	0	0.5	0.01	10	10	11.11	0.01	0.0001
Yaw Value	7	0	0.5	0.01	10	10	0.01	0.0001	—

Table 4 Summary of NASMC controller parameters and gains

An LQR controller was used as a control trial to gauge the performance of the NASMC controller. Both controllers were commanded to follow the desired waveform $\theta_d = \frac{A}{2}(1 - \cos(\frac{2\pi}{T}))$ for both pitch and yaw experiments. Where A and T are the maximum desired angle in radians and the period of the waveform in seconds, respectively.

A. Pitch 1DOF Results

The NASMC controller proved superior compared to the LQR controller as shown in Fig. 4. The NASMC controller had a mean absolute error (MAE) of $\Delta\theta^{AVG}_{NASMC} = 0.0095$ degrees and the LQR controller had an MAE of $\Delta\theta^{AVG}_{LQR} = 0.0526$ degrees. Thus, the NASMC control architecture effectively adapted to the unknown system parameters, resulting in $\frac{1}{6}$ of the MAE compared to the LQR architecture. Figure 6 shows the adaptation parameters adapting and then reaching equilibrium values.

B. Yaw 1DOF Results

The NASMC controller proved superior compared to the LQR controller in the yaw experiment as well, shown in Fig. 5. The NASMC controller had a MAE of $\Delta\psi^{AVG}_{NASMC} = 0.008$ degrees and the LQR controller had an MAE of $\Delta\psi^{AVG}_{LQR} = 0.0990$ degrees.Thus, the NASMC control architecture effectively adapted to the unknown system parameters, resulting in $\frac{1}{12}$ of the MAE compared to the LQR architecture. Figure 6 shows the adaptation parameters adapting and then reaching equilibrium values.

C. Discussion of Results

The adaptation parameters stop adapting once the combined error, s, has converged and is within the boundary layer. This fact is observed by inspecting the adaptation laws in Eqs. (12)-(14); when s converges within the boundary layer, s_Δ becomes zero, resulting in no adaptation (i.e., $\dot{\hat{h}} = \dot{\hat{a}}_1 = \dot{\hat{a}}_2 = 0$). The parameter estimates found by the adaptation laws are sufficient for error convergence, meaning that the actual system parameters are not found by the controller, only good estimates. The relationship between the combined error and parameter adaptation is also observed in the pitch 1DOF experiment. The pitch parameters adapt rapidly within the first 5.5 seconds of the experiment and then reach steady state values in Fig. 6. The pitch error over time is non-zero during these first 5.5 seconds of the experiment in Fig. 4 and then reaches near-zero error, effectively stopping the adaptation.

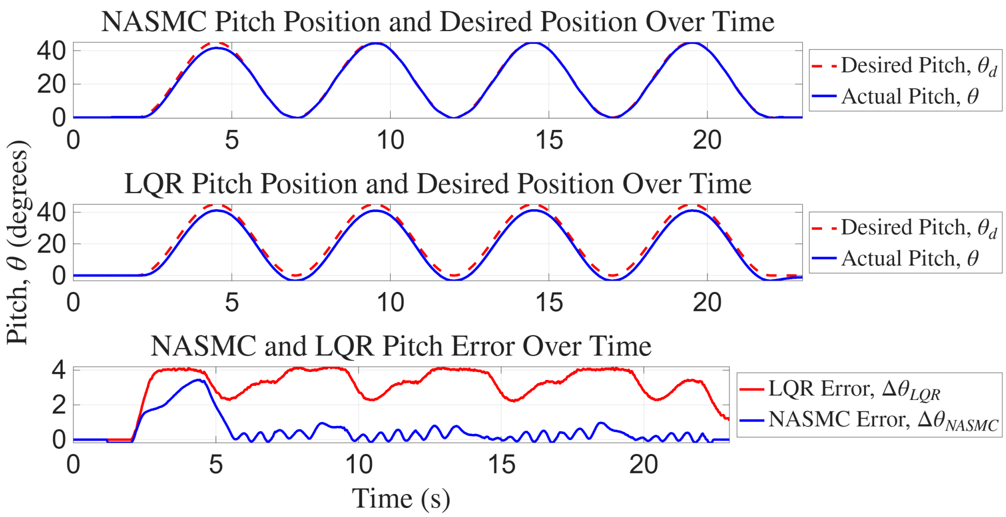

Fig. 4 Pitch 1DOF experimental results: NASMC controller vs. LQR controller

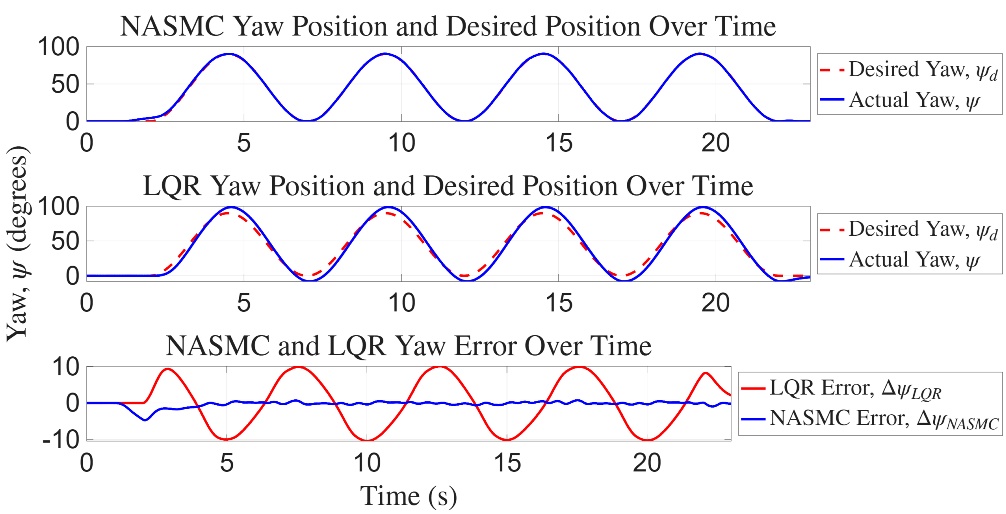

Fig. 5 Yaw 1DOF experimental results: NASMC controller vs. LQR controller

The 1DOF experiments proved NASMC to be a superior control architecture compared to LQR. The results also highlighted NASMC's ability to adapt to unknown system parameters, resulting in diminishing controller error over time. While the 1DOF results are promising, when the NASMC controller was extended to a 2DOF system, with both pitch and yaw, the results held only in simulation. The control system was unable to be proven experimentally in the 2DOF configuration. This was likely due to not having a complete understanding of the coupled dynamics between pitch and yaw. The 2DOF equations of motion used to derive the controller are documented in this paper and the reader is encouraged to critique and refine the dynamic equations to capture the missing coupling dynamics. Understanding the coupling of pitch and yaw dynamics is vital to experimentally validating this controller because, while the parameters may be unknown, the dominant system dynamics must be well understood.

The MATLAB code and Simulink model required to run the simulation, the MATLAB code and Simulink model required to run the experiment, and the experimental data collected for this paper are included in a GitHub repository at the following web URL: `https://github.com/samuelsn6399/NASMC_QuanserAero.git`.

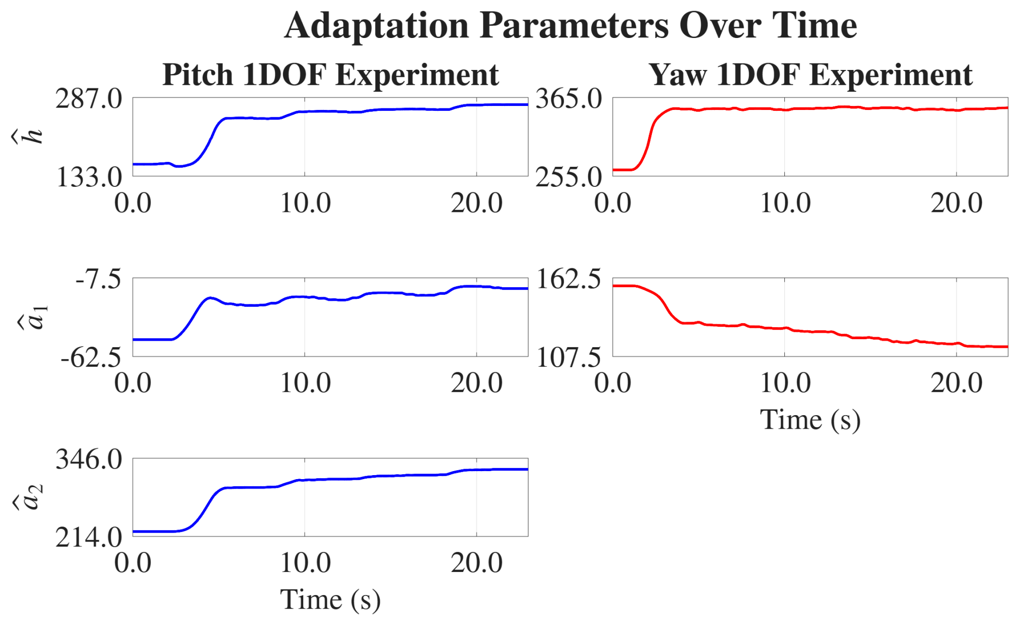

Fig. 6 NASMC parameter adaptation for both pitch and yaw experiments

VI. Conclusion

The simulated NASMC system was deployed to hardware in an attempt to experimentally validate the novel control scheme. NASMC was successfully demonstrated in 1DOF tests about the pitch and yaw axes. However, the coupled pitch and yaw dynamics were not well understood, leading to poor performance in the 2DOF configuration. Future work aiming to deploy NASMC to hardware must focus on capturing all of the dominant system dynamics.

References

[1] Mathewson, R., and Farbod, F., "Nonlinear Adaptive Sliding Mode Control With Application To Quadcopters," Master's thesis, University of Alabama in Huntsville, 2022.

[2] Alvarenga, J., and Vitzilaios, N., "Survey of Unmanned Helicopter Model-Based Navigation and Control Techniques," *Journal of Intelligent & Robotic Systems*, Vol. 80, 2014, pp. 87–138. https://doi.org/https://doi.org/10.1007/s10846-014-0143-5.

[3] Boulter, D., "Roadmap for Artificial Intelligence Safety Assurance," *Federal Aviation Administration*, Vol. 1, No. 1, 2024.

[4] Slotine, J., and Li, W., *Applied Nonlinear Control*, Prentice Hall, 1991.

[5] Slotine, J., and Coetsee, J., "Adaptive sliding controller synthesis for non-linear systems," *International Journal of Control*, 1986.

[6] Quanser, *https://www.quanser.com/products/quanser-aero/*, 2022.

[7] Dyvik, M., and Fjereide, D., "Modeling and Identification of The Quanser Aero Using A Detailed Description of Friction and Centripetal Forces," *Proceedings of the 64th International Conference of Scandinavian Simulation Society*, 2023, p. 3.